FINAL REPORT

APPLICATION OF ELECTROMAGNETIC-ACOUSTIC TRANSDUCERS FOR NONDESTRUCTIVE EVALUATION OF STRESSES IN STEEL BRIDGE STRUCTURES

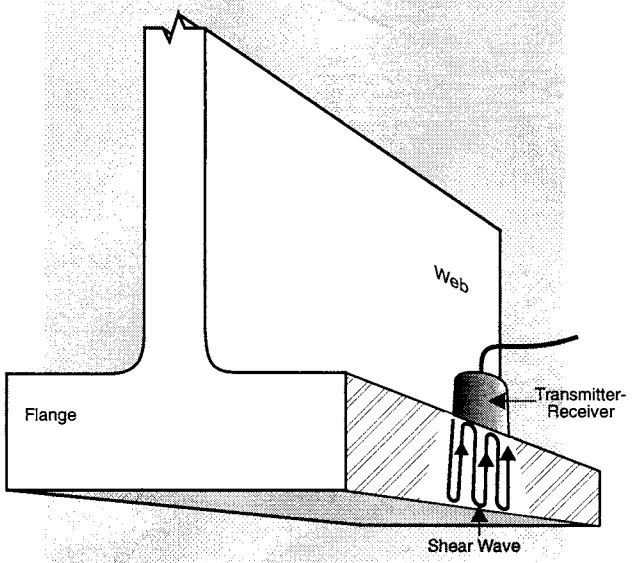

MARGARIT G. LOZEV, Ph.D.
Research Scientist

ALFRED V. CLARK, Jr., Ph.D.
Mechanical Engineer, National Institute
of Standards and Technology

PAUL A. FUCHS
Researcher, Constructed Facilities Center
West Virginia University

V · I · R · G · I · N · I · A
VTRC
TRANSPORTATION RESEARCH COUNCIL

VIRGINIA TRANSPORTATION RESEARCH COUNCIL

Standard Title Page - Report on State Project

Report No.	Report Date	No. Pages	Type Report:	Project No.:
VTRC 96-R30	April 1996	37	Final Report Period Covered:	9107-010-940 Contract No.:

Title and Subtitle
Application of Electromagnetic-Acoustic Transducers for Nondestructive Evaluation of Stresses in Steel Bridge Structures

Key Words
electromagnetic-acoustic transducers, nondestructive evaluation, residual stress, live load measurements, strain gage, ultrasonic equipment

Authors
Margarit G. Lozev, Ph.D., Alfred V. Clark, Jr., Ph.D., Paul A. Fuchs

Performing Organization Name and Address:

Virginia Transportation Research Council
530 Edgemont Road
Charlottesville, VA 22903

Sponsoring Agencies' Name and Addresses

Virginia Department of Transportation
1401 E. Broad Street
Richmond, VA 23219

Supplementary Notes

Abstract

This report presents the results of a study to (1) assess the applicability of electromagnetic-acoustic transducers for nondestructive evaluation of stresses in bridge structures and (2) evaluate the new ultrasonic instruments as an effective technique for stress surveys in bridge structures.

Field tests were performed on two bridges, one a simply supported design and the other an integral backwall bridge. Residual stress measurements were made on a vertical scanline in the web at midspan of a simply-supported bridge. Live load measurements were made by determining the normalized change in arrival times of surface waves propagating between two transducers mounted on the bottom flange. Good agreement between strain gage and ultrasonic data was obtained, both for the time-history of strain and also for the equivalent stress range.

The ultrasonic equipment for live load measurements is portable and easily installed. Unlike strain gage installation, ultrasonic measurements could be made without paint removal.

FINAL REPORT

APPLICATION OF ELECTROMAGNETIC-ACOUSTIC TRANSDUCERS FOR NONDESTRUCTIVE EVALUATION OF STRESSES IN STEEL BRIDGE STRUCTURES

Margarit G. Lozev, Ph.D.
Research Scientist

Alfred V. Clark, Jr., Ph.D.
Mechanical Engineer, National Institute of Standards and Technology
Boulder, CO 80303

Paul A. Fuchs
Researcher, Constructed Facilities Center, West Virginia University
Morgantown, WV 26506

Virginia Transportation Research Council
(A Cooperative Organization Sponsored Jointly by the Virginia Department of Transportation and the University of Virginia)

Charlottesville, Virginia

April 1996

VTRC 96-R30

ABSTRACT

The report presents the results of a study to (1) assess the applicability of electromagnetic-acoustic transducers for nondestructive evaluation of stresses in bridge structures and (2) evaluate the new ultrasonic instruments as an effective technique for stress surveys in bridge structures.

Field tests were performed on two bridges, one a simply-supported design and the other an integral backwall bridge. Residual stress measurements were made on a vertical scanline in the web at midspan of the simply-supported bridge. Live load measurements were made by determining the normalized change in arrival times of surface waves propagating between two transducers mounted on the bottom flange. Good agreement between strain gage and ultrasonic data was obtained, both for the time-history of strain and also for the equivalent stress range.

The ultrasonic equipment for live load measurements is portable and easily installed. Measurements can be made without paint removal, unlike strain gage installation.

FINAL REPORT

APPLICATION OF ELECTROMAGNETIC-ACOUSTIC TRANSDUCERS FOR NONDESTRUCTIVE EVALUATION OF STRESSES IN STEEL BRIDGE STRUCTURES

Margarit G. Lozev, Ph.D., Research Scientist
Alfred V. Clark, Jr., Ph.D., Mechanical Engineer
Paul A. Fuchs, Researcher

INTRODUCTION

Virginia has about 12,000 state-maintained bridges, 1,321 of which are classified as structurally deficient.[1] A bridge with a structurally deficient rating has structural problems that restrict it to light vehicle use, requires rehabilitation to remain open, or is closed and beyond repair. It would not be economically feasible to replace all of these structures. In the late 1970's John W. Fisher studied the cracking in structurally deficient bridges.[2] He discovered that all cracks removed for examination originated at a porosity or entrapped piece of slag in a region of high residual tensile stress from weld shrinkage. To assess the criticality of these cracks he applied a fracture mechanics model and considered the contribution of residual stresses, live load stresses, and dead load. Residual stresses are "locked into" the weld during welding. Live loads are applied stresses due to passage of vehicle traffic. Vehicle traffic on bridges generally causes stress cycles of varying amplitude in the structure. These stress cycles are normally low, below 14 MPa (2 ksi).[3] To analyze these data, the stress cycles are placed in histograms with typical increments of ± 3.5 MPa (± 0.25 ksi) and converted to an equivalent constant amplitude stress cycle. These stresses are the cause of fatigue cracks in bridges. Fatigue cracks may disable a bridge or possibly cause structural failure. Fisher's analysis showed that it is desirable to remove the cracks promptly.

Currently, the main nondestructive evaluation (NDE) methods of measuring residual stress include x-ray[4] and neutron diffraction.[5] Unfortunately, these techniques are limited to laboratory applications and to the measurement of stress at or near the metal surface. Ultrasonic methods based on acoustic Barkhausen noise,[6] magnetically induced velocity changes, and magneto-acoustic emission[7] are either in an early developmental stage or have severe limitations.

The most common method of measuring stress with ultrasound is based on the acoustoelastic effect – the variation of ultrasonic velocity due to the presence of stress.[8] For small changes in the acoustic wave's velocity (less than 1%), a general relationship between the measured velocity of an acoustic wave and stress is linear and can be described by the relation

$$V = V_0 + K\sigma \qquad (1)$$

where V_0 is the velocity of the wave in an unstressed medium, σ is the stress, and K is an acoustoelastic constant. The acoustoelastic effect is most readily observed when stress is applied to a material. In this way the applied stress (change in stress from a previously known state) can be measured. Ultrasonic techniques measure stress in a surface layer, as well as in the bulk of a component. The velocity change is proportional to the average stress in the region through which the waves propagate. The ultrasonic instrumentation is convenient to use, quick to set up, and free of radiation hazards. Disadvantages of the ultrasonic approach include low spatial resolution, susceptibility to competing sources of velocity shifts due to microstructural effects and temperature variations, and necessity for very precise time measurements.[9]

Acoustoelastic theories and experiments are presented for ultrasonic through-thickness residual stress measurements using shear wave birefringence (difference of velocity).[9] In an isotropic, stress-free material, shear waves will travel at the same velocity. Stress application introduces elastic anisotropy to the solid materials and splits the propagating shear wave into two orthogonally polarized components. The shear wave birefringence technique is sensitive to the difference of principal stresses rather than the sum. The normal incidence birefringence method using various noncontact electromagnetic-acoustic transducers (EMATs) is favored for its relatively high sensitivity. A measurement of resonant frequencies and phase shifts obtains the acoustic birefringence and determines the principal stresses.[10] A good agreement with the theory is found. The use of a magnetostrictive-type EMAT to excite and detect the surface-skimming shear-horizontally polarized wave has been proposed.[11] The measured velocity potentially indicates the surface stresses, being independent of the microstructure.

Currently, applied stress or live load monitoring is accomplished by bonding an array of strain gages to a bridge member. However, strain gages can be time-consuming to install because paint removal is required. In addition, lead-based paint removal is a safety hazard. Under the sponsorship of the Federal Highway Administration (FHWA), the Constructed Facilities Center (CFC) of West Virginia University, in collaboration with the National Institute of Standards and Technology (NIST) at Boulder, jointly developed an ultrasonic fatigue loading indicator for bridges to measure live load stresses. The indicator has two sections. The first section measures the applied stress, and the second processes the data and determines the number of constant amplitude fatigue cycles seen by the structure.[12] This device uses EMATs to generate Rayleigh (surface) waves in the flanges of I-beams.[13] An instrument for time-of-flight Rayleigh wave velocity measurements and applied stress applications has been successfully demonstrated.[14]

PROBLEM STATEMENT

Quantitative measurement of residual and applied or live-load stresses is needed to adequately determine the safety of bridge structures and decide which structures need rehabilitating or replacing.

At present, there are systems to measure residual and applied stress using x-ray, neutron diffraction and strain gauges. These techniques are labor-intensive, time-consuming and hazardous. In many cases, the instruments cannot be used in the field and are not reliable for long-term or continuous monitoring.

A technique that measures residual and applied stress in a bridge with minimal installation time and minimal safety precautions is needed. Noncontact ultrasonic techniques could measure stresses with good resolution, and are a possible solution to this problem.

POTENTIAL BENEFITS

The potential direct benefit of this study will be the implementation of NDE methods for assessing stresses in steel bridge members, which will increase the reliability of inspections and the safety of bridge structures.

PURPOSE AND SCOPE

The objectives of this project are (1) to assess the applicability of electromagnetic acoustic transducers for NDE of stresses in bridge structures, and (2) to evaluate the new ultrasonic instruments as an effective technique for stress survey in bridge structures. This will be a proof-of-concept field experiment to demonstrate the feasibility of measuring stresses in steel bridges using noncontact ultrasonic techniques.

ELECTROMAGNETIC-ACOUSTIC TRANSDUCERS: PRINCIPLE OF OPERATION

The basic EMAT consists of a coil and magnet. In operation a power amplifier is used to generate a short-duration toneburst of current in the coil, typically at megahertz (MHz) frequencies. When the coil is close to the surface of a conducting material it generates eddy currents in the surface, which mirror the pattern of wires in the coil. The magnet causes a magnetic induction B in the material as well. A force F (Lorentz force) is induced on the material given by the vector product

$$F = jxB \qquad (2)$$

where j is the eddy current density. This is the same force which runs electric motors. A current flows through the wires in the motor in reaction to the magnetic fields of the motor magnets, exerting a force on the windings. In the case of the EMAT, the force is exerted at the surface (acts over the skin depth of eddy currents). Because the force is time-varying (the coil current

varies at MHz frequencies) the surface is not in static equilibrium and a propagating stress wave is set up.

EMATs require no couplant to transmit sound into the material under investigation. However, they are intrinsically less efficient than the most common type of ultrasonic piezoelectric transducer. In general piezoelectric transducers are more complicated to fix to the surface for reliable measurements. Since the EMATs used in this study employed permanent magnets, they were relatively easy to use even on the vertical surfaces of girder webs.

EMATs can work with a one millimeter clearance (lift-off) from the surface, and can generate and receive sound through modest amounts of rust and scale. One of the issues in this project was to evaluate their operation on painted bridge girder surfaces.

This project used different designs of EMATs. For live load monitoring the EMAT coil was in the form of a meanderline (serpentine winding). The period of the windings was chosen to match that of a Rayleigh wave, typically at 1 MHz (Figure 1).

The second design was used for both live load and residual stress measurements. It consisted of two counterwound "racetrack" coils placed side-by-side. A copper shield was placed over the coils. The shield had an aperture equal to the size of the side-by-side straight legs of the coils. The eddy currents below the aperture were in the form of straight lines parallel

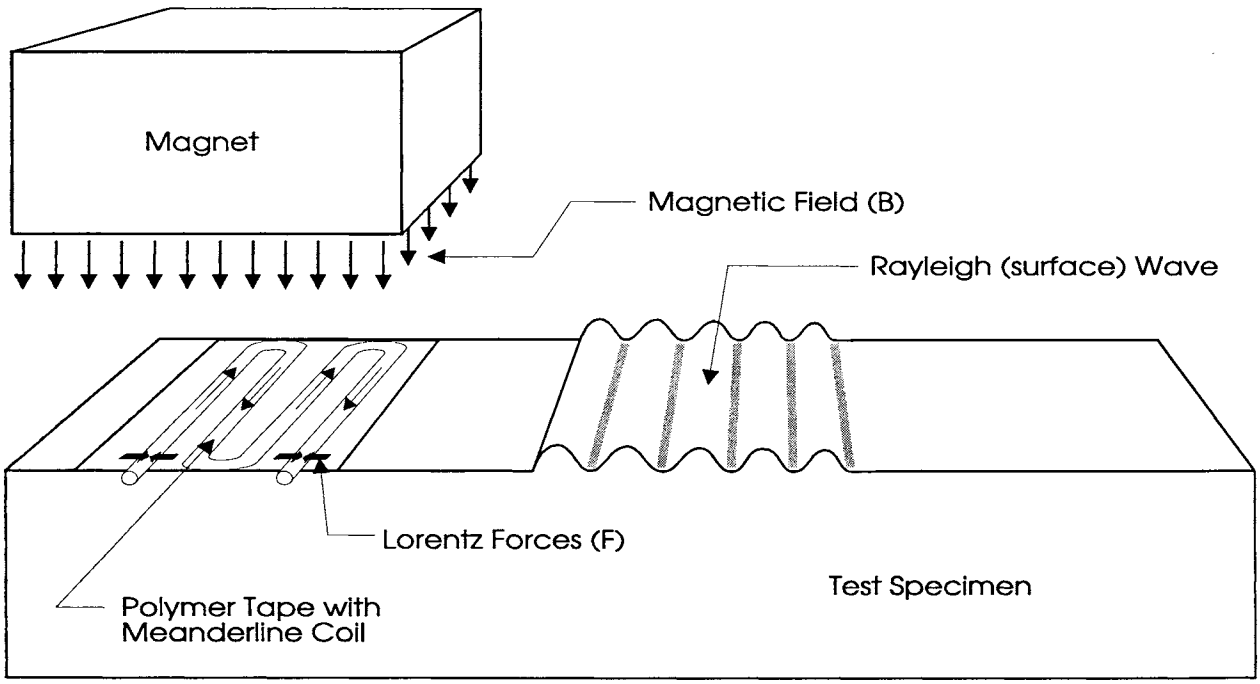

Figure 1. EMAT design for Rayleigh (surface) wave generation.

to the surface. The magnetic induction acts normal to the surface so the resulting shear wave has polarization perpendicular to the wires (Figure 2). We tested three such EMATs. Two were tuned for 2 MHz operation and one for 4 MHz. These EMATs were mounted in a tube and a magnetic holder to allow rotation in five degree increments.

A third type of EMAT was designed and a prototype built before the field test. This device consisted of a loop of wires under a periodic array of permanent magnets. The magnet spacing corresponded to the period of a surface-skimming shear wave at 0.5 MHz in steel. This EMAT was mounted in a fixture to allow rotation in 90 degree increments. The advantage of this type of EMAT is that it allows determination of bending stress regardless of variation in material properties (texture). The theory behind this is given later.

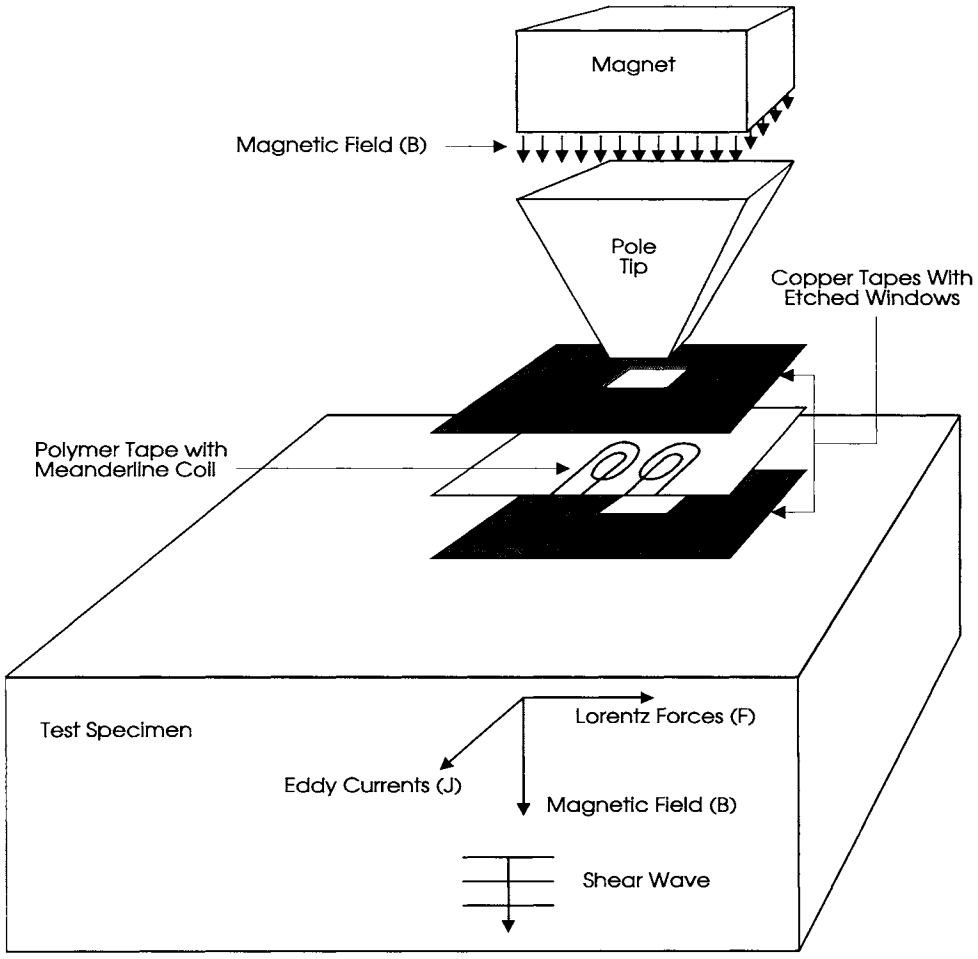

Figure 2. EMAT design for shear wave generation.

METHODS

Instrumentation and Procedures

Applied (Live Load) Stress Measurements

For live load measurements a sensor head was constructed at CFC (with input from NIST) consisting of a transmitting and a receiving EMAT. A low-noise preamplifier was connected to the receiver. Figure 3 shows the EMATs housed in aluminum boxes and connected to each other by spring-loaded rods. When placed on the surface of a steel girder, the EMATs move relative to each other due to strains from live loads.

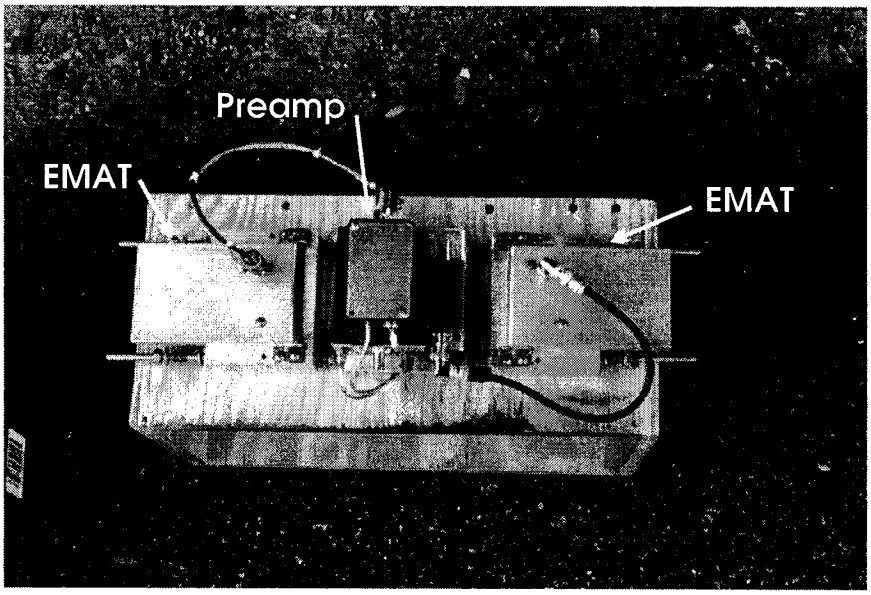

Figure 3. Sensor head for Rayleigh wave EMAT.

In the unstressed state, the transit time $T = D/V$, where D is the distance between centers of the EMATs and V, is the wave velocity. Stress causes both the distance and the velocity to change. The percent change dD/D is the strain ϵ in the girder. The percent change in velocity is due to the acoustoelastic effect, which states that dV/V is proportional to stress.[8]

For live loading the bending stress is proportional to ϵ. Hence

$$\frac{dT}{T} = C_s \epsilon \qquad (3)$$

where C_s is a dimensionless constant pertaining to surface-wave operation. For typical bridge steels (A-36, for example) we have measured C_s to be about one.[15]

The equipment for the live load measurement developed at CFC is portable and is housed in a small suitcase which was suspended from the girder under test (Figure 4). A custom-made pulser delivers about 10 watts at the given repetition rate 8 Hz to the transmitting EMAT. The output of the receiver (after the gain of the preamplifier) is digitized for signal processing which determines the transit time T between EMATs. Figure 5 is a block diagram of the instrument.

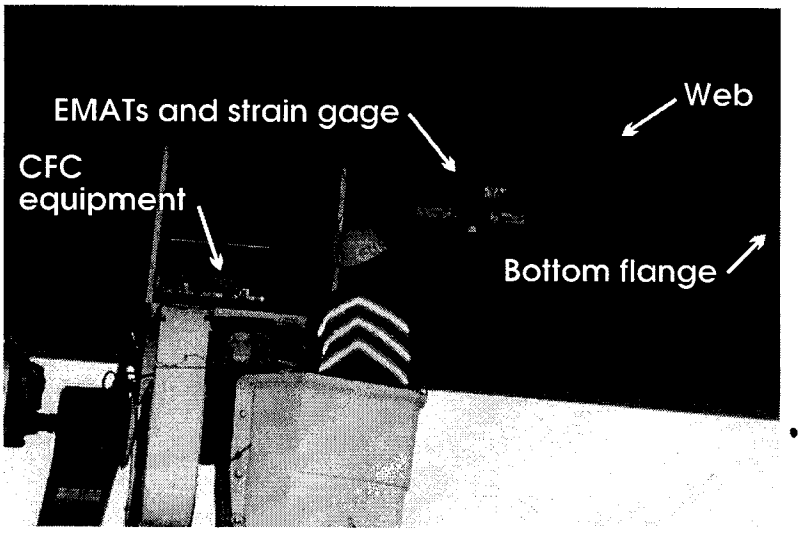

Figure 4. Fatigue loading indicator and the sensor head on the beam.

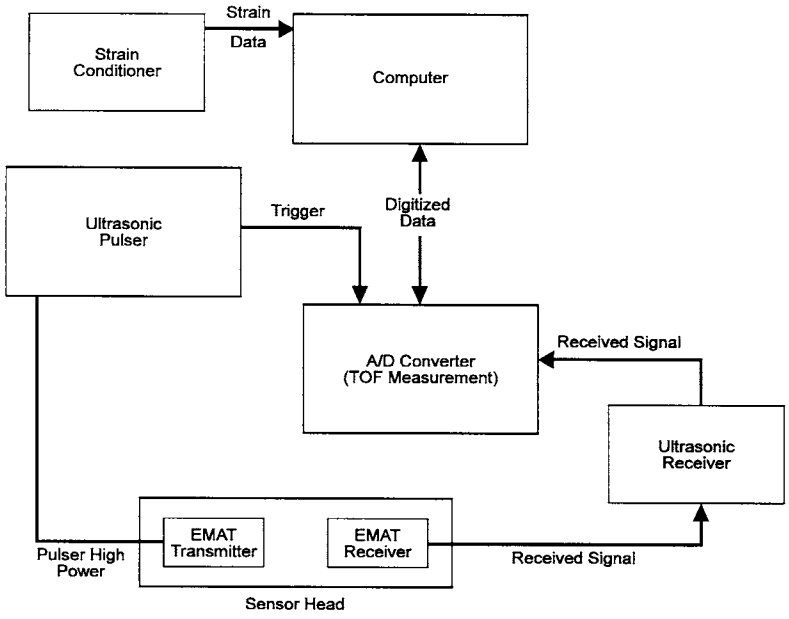

Figure 5. Ultrasonic applied stress system block diagram.

In operation the sensor-head is usually placed on the bottom of the bottom flange of a girder where the live load bending stress will be maximum (Figure 4). The pulser generates tonebursts at either 0.5 or 1.0 MHz, depending upon which design of EMAT is used. The transmitting EMAT generates a surface wave with amplitude decaying exponentially with depth, which propagates along the flange (Figure 6). The time for the Rayleigh wave to travel from the transmitter to the receiver is measured digitally. (The received waveform is digitized at 50 MHz and the time-of-flight is determined with algorithms within a computer.) The initial time-of-flight measurement is taken as the normalizing time T. The system will then continue to sample time-of-flight measurements at about 8 Hz. The time-of-flight data is converted to values of applied stress and stored in a computer. Both EMAT and strain gage measurements are made at the same point in time for comparison purposes.

Live load stresses were also measured with the shear wave EMAT. This device sends sound through the flange in the thickness direction (Figure 7). There are generally several echoes as the wave propagates back and forth in the flange. These are detected by the EMAT and processed by the electronics described above.

The stresses measured with EMAT were compared with electrical resistance strain gages (350 ohm). Strain gages were bonded to the bottom of the bottom flange surface adjacent to the EMAT. Strain gages were connected to the CFC system.

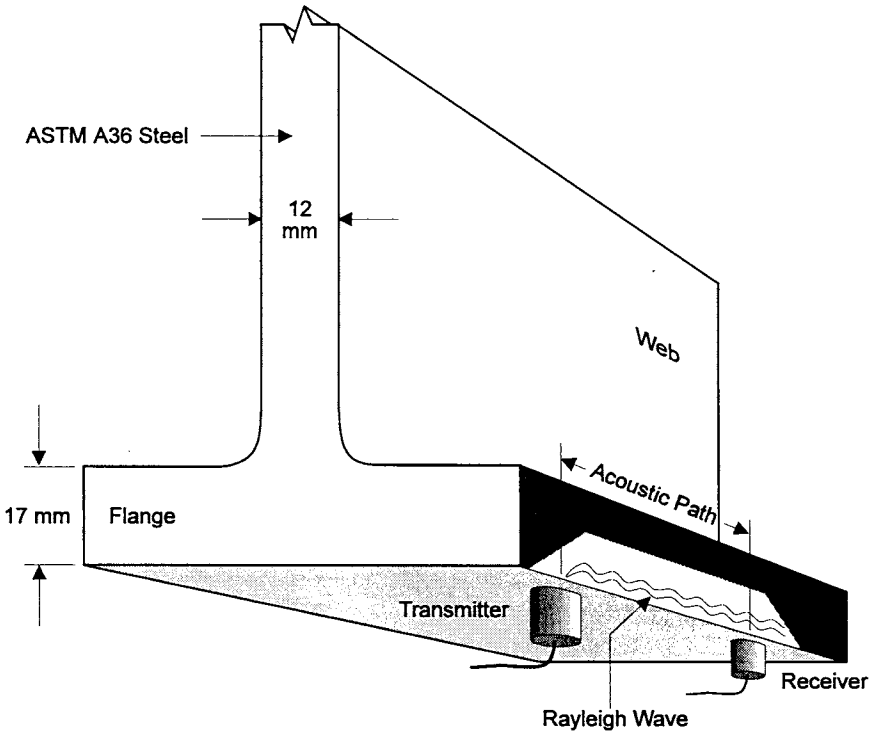

Figure 6. Rayleigh wave propagation on the bottom flange of the Rte. 681 bridge over I-64.

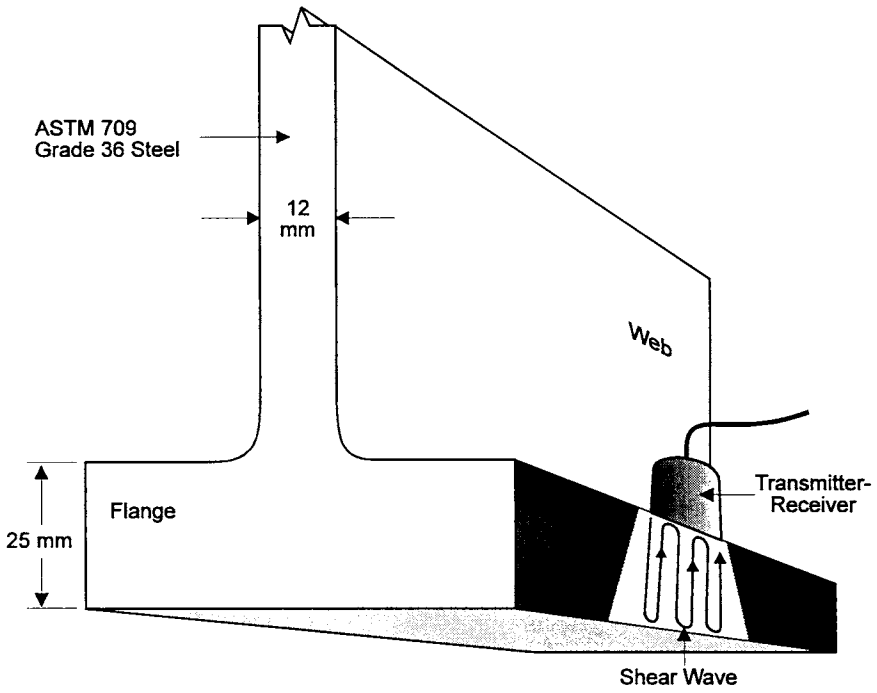

Figure 7. Shear wave propagation on the bottom flange of the Rte. 257 bridge over I-81.

Residual (Dead Load) Stress Measurements

In general dead load (and residual stress) measurements are more difficult. Live load measurements are referenced to the static state, which is easy to determine (no traffic on bridge). Dead load measurements are referenced to an absolute zero stress state (which may not even exist anywhere on a bridge). Dead load stresses result from self-weight. Residual stresses come from fabrication.

The shear wave EMAT was used to measure dead load and residual stresses on a steel bridge structure. Design, fabrication, tuning, and calibration of the shear wave EMATs were performed at the Materials Reliability Division, NIST, Boulder. The performance characteristics of the EMATs and the preamplifiers were evaluated in laboratory experiments. The NIST stress measurement capability was transferred to the VTRC to measure stresses in bridge members. Figure 8 is a close-up of the shear wave transducer.

For this application we employed a state-of-the art ultrasonic instrument which generated the high-current toneburst to drive the EMAT, amplified the output of our custom preamplifier, gated out a selected echo, and measured either the transit time or phase of the selected echo. Figure 9 is a block diagram of the setup used for the residual stress measurement. The signal arriving at the transducer is of the form $Asin(\omega t+P)$ where $P = \omega T$ is the phase in the wave due to transit time T and ω is the radian frequency. In our instrument this signal was mixed with a

reference signal $Asin(\omega t)$ in the "phase" channel and with signal $Acos(\omega t)$ in the "quadrature" channel. After low-pass filtering the voltages in these channels are respectively $V_p = AsinP$ and $V_q = AcosP$. These are digitized and the computer calculates the phase from $P_m = arctan(Vp/Vq)$. Here the subscript m denotes a measured value. The computer algorithm calculates P_m within multiples of 2π.

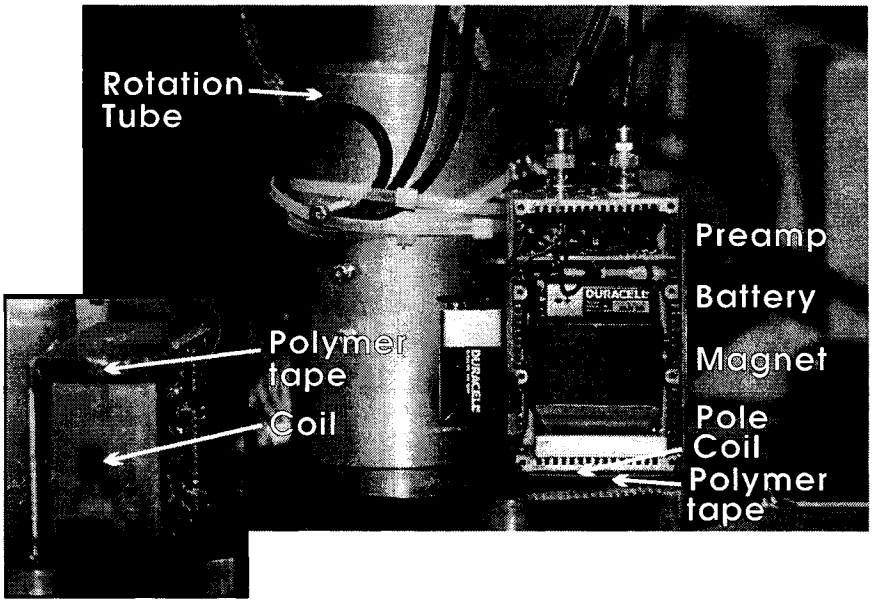

Figure 8. Close-up of shear wave transducer.

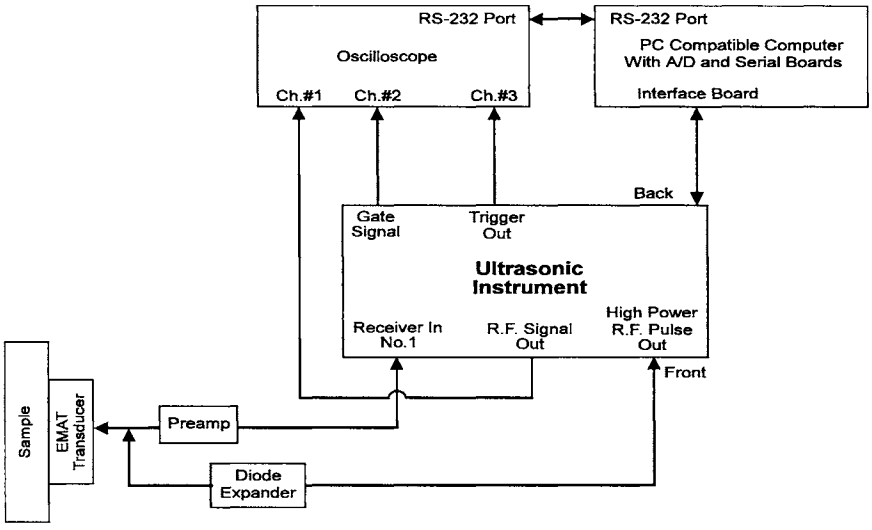

Figure 9. Block diagram of the setup for residual stress measurements.

In the simplest form of operation, it is known *a priori* that the principal stresses are parallel and perpendicular to the rolling direction. The EMAT is oriented to generate a shear wave polarized in, for example, the rolling direction, and the phase measured. The operation is then repeated for the orthogonal direction. The percent difference in phase dP/P is the negative of dV/V (since the waves pass through the same thickness).

The quantity dV/V is called the acoustic birefringence B. For this case we have the relation

$$B = B_0 + C_a(\sigma_r - \sigma_t) \qquad (4)$$

where σ_r is the normal stress in rolling direction, σ_t is the normal stress in the transverse direction and C_a is the stress-acoustic constant. For a typical bridge steel (A-36) we measured $C_a = -1/(10^5 \text{ MPa})$. B_o is the value of B in the unstressed state and is assumed constant throughout the material. This unstressed birefringence is nonzero because rolling gives rise to small differences in shear moduli in rolling and transverse directions. Here

$$B = \frac{2(V_r - V_t)}{V} \qquad (5)$$

From the definition of birefringence and relations between phase, transit time, and velocity, we have

$$B = \frac{(V_f - V_s)}{V} = \frac{(P_s - P_f)}{P} \qquad (6)$$

where f denotes the fast direction and s denotes the slow direction.

We obtain the difference in phases for one chosen frequency by orienting the transducer to propagate waves in fast and slow directions and having the instrument measure P_m in both orientations. We then take the difference in P_m for these directions to obtain $P_s - P_f$.

To determine the "absolute" phase P we use the instrument in another mode. Here it sweeps the frequency of operation over a selected range (typically 0.5 MHZ) and measures the phase at each frequency (in software the computer keeps track of multiples of 2π as frequency is swept). The computer then calculates the phase slope $dP/d\omega = T$ so the transit time is obtained. Then for the chosen frequency we have $P = \omega cT$ in equation (6).

In general there will be shear stresses in addition to normal stresses. Then the orientation of pure shear waves will rotate by angle Θ from the rolling direction. The theory is given in the

Appendix. It will be necessary to determine this orientation and measure the corresponding birefringence. Then

$$B\cos(2\theta) - B_0 = C_a(\sigma_{xx} - \sigma_{yy}) \qquad (7)$$

As mentioned previously, an EMAT for surface-skimming shear waves was constructed but not ready for the field test. This device can be used to measure arrival times of waves propagating in rolling and transverse directions. The normalized difference in times dT/T is proportional to the difference in principal stresses

$$\frac{dT}{T} = \left(\frac{1}{2\mu}\right)(\sigma_1 - \sigma_2)\cos(2\Phi) \qquad (8)$$

where μ is shear modulus and Φ is the angle between rolling and principal stress directions. Consequently when measurements are made away from bearings (normal stress in vertical direction vanishes) dT/T gives the bending stress. This is true regardless of texture variations (note that B_o does not appear in the above equations). The relation is true even if the material has been plastically deformed.

The Value of Measurement of Stresses

Suppose there is a vertical crack in the girder and some estimate of structural safety is desired. Fracture mechanics provides a means for doing this. The stress-intensity factor K_I (a measure of the crack-driving force) can be calculated from

$$K_I = \int_0^a h(y)\,\sigma_{xx}(y)\,dy \qquad (9)$$

where a is crack length and the weighting function $h(y)$ is proportional to the value of K_I for concentrated force at location x on the crack face. For simple geometries $h(y)$ is given in the literature. The σ_{xx} are bending stresses at the crack before crack formation (before redistribution of stress by the crack). If K_I is greater than the critical stress intensity factor K_{Ic} a brittle fracture occurs. In equation (9) σ_{xx} is total stress due to dead loads, live loads, and residual stresses. The latter can be caused by cambering, welding, shrinkage of a concrete deck, rolling of a girder, etc.

As an example of the use of equation (9), it has been used to show (mathematically) that sufficient compressive residual stress in the web will arrest a brittle fracture. In fact the compression may even stop fatigue crack growth (for large enough compression). A finite element analysis has been performed to determine stresses in a cracked beam. The crack

redistributes stress locally over a distance of about one beam depth. At greater distances from the crack the stresses are what they were prior to cracking.[19]

To evaluate the safety of a cracked beam it is proposed to determine the total stress state at about one beam depth from the crack and then use the equation above to determine K_I as function of crack depth. This is simulated in the test of the Rte. 691 bridge over I-64.

RESULTS AND DISCUSSION

Laboratory Tests

To ensure the validity of the data, several issues were addressed before field testing:

- The orientation of the acoustic axes needed to be determined. The shear stress in the bridge girders could cause the "fast" and "slow" wave directions to rotate. One criterion for good data is that the phase or time-of-flight (TOF) data should repeat at 180 degree intervals as the EMAT is rotated.

- Paint severely reduces signal amplitude. A means to suppress this effect would be desirable.

- Previous tests at NIST had shown that "clean" acoustic signals were required if the necessary precision in birefringence measurement was to be obtained. That is, we need discrete echoes with minimal coherent "noise" on the signal baseline.

Several procedures were adopted to address these issues. We first developed a method to determine the orientation of "fast" and "slow" axes. The ultrasonic instrument was operated in the "relative time" mode. This allows the operator to view changes in transit time of the wave in real time as the EMAT is rotated in the holder. The computer monitor displays the arrival time changes and the operator determines when the EMAT is polarized in fast and slow directions. The "relative phase" mode is then used to measure the difference dP in phase in these directions. A frequency sweep is made to determine the absolute phase P. The birefringence B is then determined from

$$B = \frac{dP}{P} \qquad (10)$$

where dP = (phase in slow direction) - (phase in fast direction).

These data were measured with two different EMATs using a magnetic holder. With one we obtained data where the TOF at zero (rolling direction in specimen) and 180 degrees agreed quite well, but the 90 and 270 degree data were different. This is probably due to a slight taper

in specimen thickness in the 90 degree direction, coupled with an offset in the center of the EMAT aperture. In effect, the EMAT "wanders" because its center does not coincide with the center of rotation. With the other EMAT reproducible data were obtained for all orientations. We used this as the primary EMAT in the field to measure fast and slow directions.

We also performed experiments to characterize the effect of paint, operating frequency, magnetic artifacts, measurement echo, and lift-off. A steel specimen spray-painted on one side had areas of good and weak acoustic signals. When the paint was removed in the weak signal areas the signal improved. Also, adding a thin layer of spray adhesive over the paint at weak signal areas helped.

Possibly the paint has an acoustic impedance close to steel. Some of the wave incident on the steel-paint interface is transmitted into the paint. Depending upon the frequency and thickness, the signal from the paint layer may be out of phase with the (desired) signal reflected from the paint-steel interface. This destructive interference could reduce the signal amplitude. Addition of the spray adhesive produces another layer which either absorbs some signal from the paint or produces partial reflections to cancel out the paint signal. The effect of paint needs to be more fully investigated.

Testing showed that our 2 MHz EMAT consistently gave better signals than our 4 MHz EMAT. The baseline with the 2 MHz device was cleaner and the birefringence measurements satisfied consistency checks. These consist of measuring birefringence with different echoes, and also on the same echo but with different gate widths (varying which part of the echo the instrument samples). Consistency checks were also part of the routine measurement during the field test.

Apparently magnetic artifacts and lift-off up to 0.5 mm (0.02 in) do not significantly alter the measurements. Poor signals were generated on specimen surfaces which were machined (hand grinder/Blanchard grinder) to eliminate surface roughness. No significant change was seen for various measurement echoes, although the fourth echo was slightly more consistent when compared with the third and fifth echoes.

In the laboratory, arrival times of waves propagating in rolling and transverse directions in steel specimens were measured with a surface-skimming shear wave device. The precision obtained was of the order of parts in 10^4, not quite good enough for the intended (residual stress) application. An improved fixture was designed but not ready in time for the field test.

Field Tests

Field tests were conducted on two bridges, one over I-64 and the other over I-81. The first was a four-span, four-girder simply-supported design. The second was an integral backwall bridge which had been previously instrumented by VTRC personnel as part of another project.[20]

Case 1: Rte. 691 Bridge over I-64

Applied (Live Load) Stresses

The Rte. 691 bridge over I-64 is a slab-on-girder composite structure with four A36 steel girders. The bridge is located on Rte. 691 west of Charlottesville, VA and passes over I-64. The testing was performed in the right-most lane in the west-bound direction. The span length was approximately 24 m (75 ft) and the center of the span was 5 m (16 ft) above the road surface Figure 10 shows the elevation and plan of the bridge. Live load measurements were performed at midspan on the two easternmost girders. A 11400 kg (25 ton) vehicle was used to apply stress to the structure. Strain gages were mounted on each of the two girders used for testing for comparison to the ultrasonic measurements. The girders were painted with lead-based paint, which had a thickness of about 0.20-0.25 mm (0.008-0.01 in) on the flange.

The Rt. 691 bridge was tested under controlled conditions. Traffic on the structure was limited to a test vehicle, which was driven over the bridge at various speeds to evaluate dynamic measurements with the ultrasonic applied stress measurement system. Representative data are shown in Figures 11 and 12. The strain gage data and EMAT data are artificially offset in the figures so the two plots can easily be distinguished.

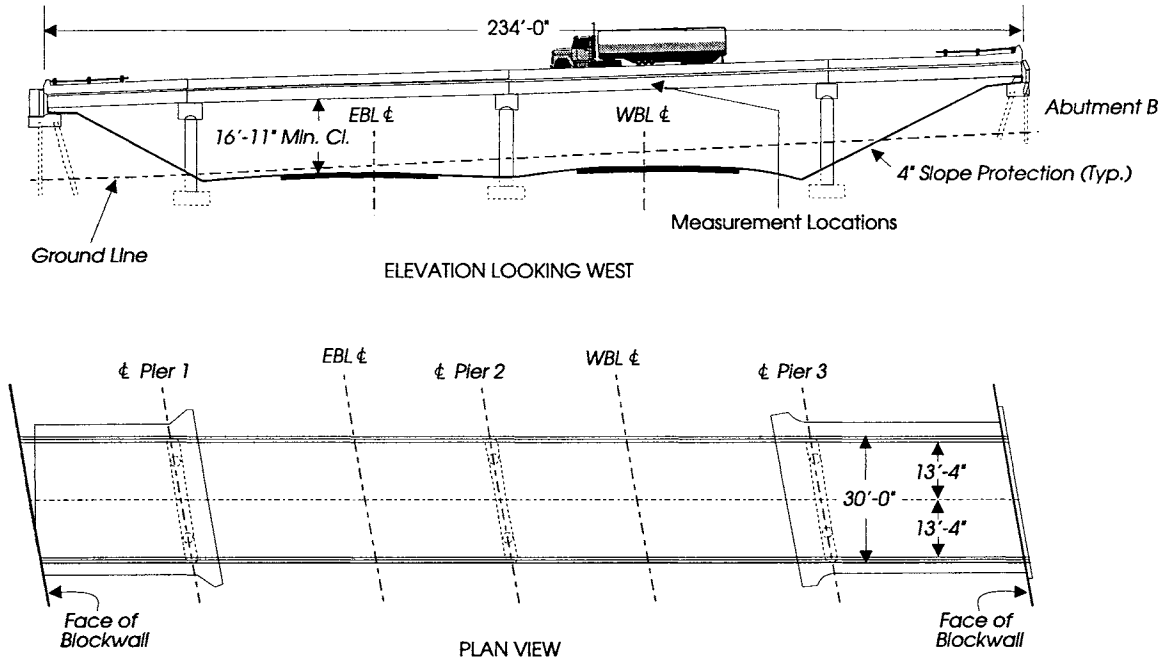

Figure 10. Elevation and plan for the Rte. 691 bridge over I-64.

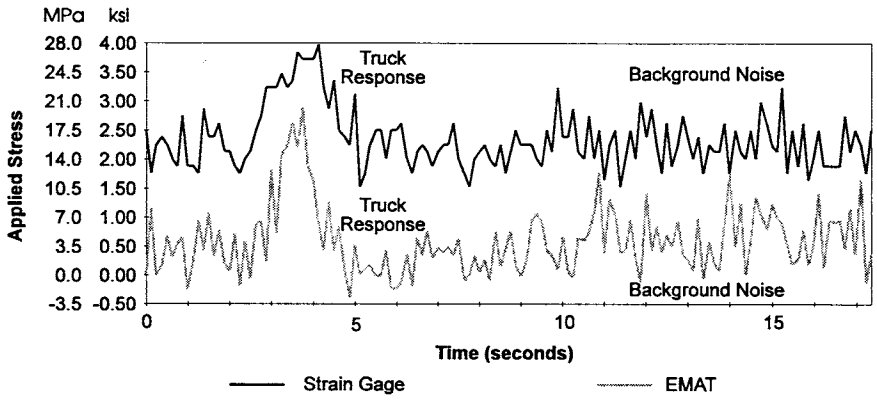

Figure 11. Data from test vehicle traveling at 40 kmph (25 mph).

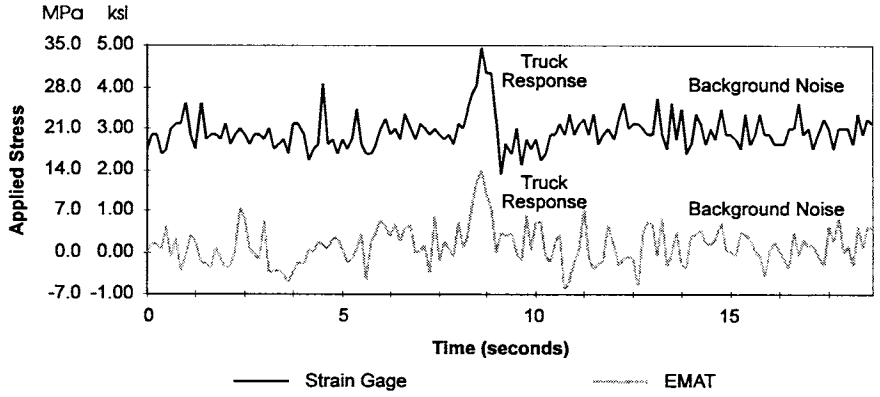

Figure 12. Data from test vehicle traveling at 89 kmph (35 mph).

The EMAT and strain gage data can be compared by examining the results of cycle counting the data. The raw data can be processed with a conventionally accepted technique of rainflow cycle counting.[16-18] The results of the rainflow cycle counts can be placed in a histogram for analysis. This histogram can be processed with an algorithm based on Miner's rule to determine the equivalent stress range represented by the particular histogram.[16] Figure 13 is a stress histogram from the data in Figure 12.

Several sets of data collected from the I-64 bridge were processed with a rainflow cycle counting algorithm to produce stress histograms. The equivalent stress range represented by each histogram was then determined. Table 1 shows the value of stress range S_{re} calculated for both the EMAT and strain gage data along with the corresponding percent error. Nine sets of data are given as a result of a test vehicle traveling at various speeds. A threshold of 7.0 MPa (1 ksi) was used to eliminate counts of stress cycles below the noise level.

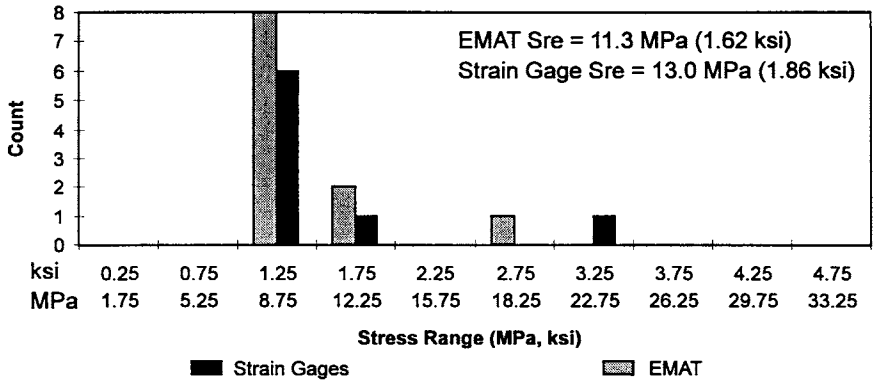

Figure 13. Stress histogram using data from Figure 12.

Table 1. Results of Cycle Counting

Speed	Run	EMAT S_{re} MPa (ksi)	Strain Gage S_{re} MPa (ksi)	% Error
8 kph (5mph)	1	13.2 (1.88)	13.1 (1.87)	0.5
8 kph (5mph)	2	13.2 (1.89)	14.0 (2.00)	5.5
8 kph (5mph)	3	11.3 (1.61)	10.6 (1.51)	6.6
40 kph (25mph)	1	13.0 (1.85)	11.9 (1.70)	8.8
40 kph (25mph)	2	13.6 (1.94)	12.1 (1.73)	12.1
40 kph (25mph)	3	13.0 (1.85)	11.7 (1.67)	10.8
89 kph (55mph)	1	12.5 (1.78)	13.0 (1.86)	4.3
89 kph (55mph)	2	11.3 (1.62)	13.0 (1.86)	12.9
89 kph (55mph)	3	13.1 (1.87)	13.2 (1.88)	0.5
% Error Average				6.9

The results of the applied stress measurements can be applied to various forms of analysis, such as determination of the fatigue cycles seen by a structure. For the particular data sets given, the stress histograms showed about a 10% difference between the EMAT and strain gage data. These histograms resulted from data only over a short period of time and represent only a small sample set. However, they did show that the EMAT system was capable of performing applied stress measurements on actual bridge structures which could closely track results from a conventional strain gage.

Typical noise for the EMAT system results in stress uncertainty of about 7.0-10.5 MPa (1.0-1.5 ksi). The effective sampling rate was about 8 Hz, which resulted from 50 signal averages per measurement. The pulse repetition rate was about 400 Hz. The strain gage noise was approximately 3.5-7.0 MPa (0.5-1.0 ksi), slightly lower than the EMAT noise. The Rayleigh wave signals through the paint on actual bridge members were very good, and the noise measured in the field experiments was essentially the same as in the laboratory when simulating field girder surface conditions (Figure 14). However, an improvement in the noise would be beneficial. Also, the response time of the system must be improved.

One important measurement during the field test was the calibration constant C_s. Extensive laboratory testing was performed to show that an off-line calibration could be used to make field measurements.[16-18] This calibration was determined in the field for comparison to laboratory results. The field calibration for C_s was approximately 0.9. The laboratory calibration for C_s was 1.01. Given the technique used for determining the field calibration constant, the result shows that the calibration for field and laboratory were close.

Residual (Dead Load) Stresses

The Rte. 691 bridge test was informative about equipment reliability and the need for ease of handling and transport. This test required a snooper truck to get to the girders. A shelf had to be hung from the side of the bucket for the operator's instruments.

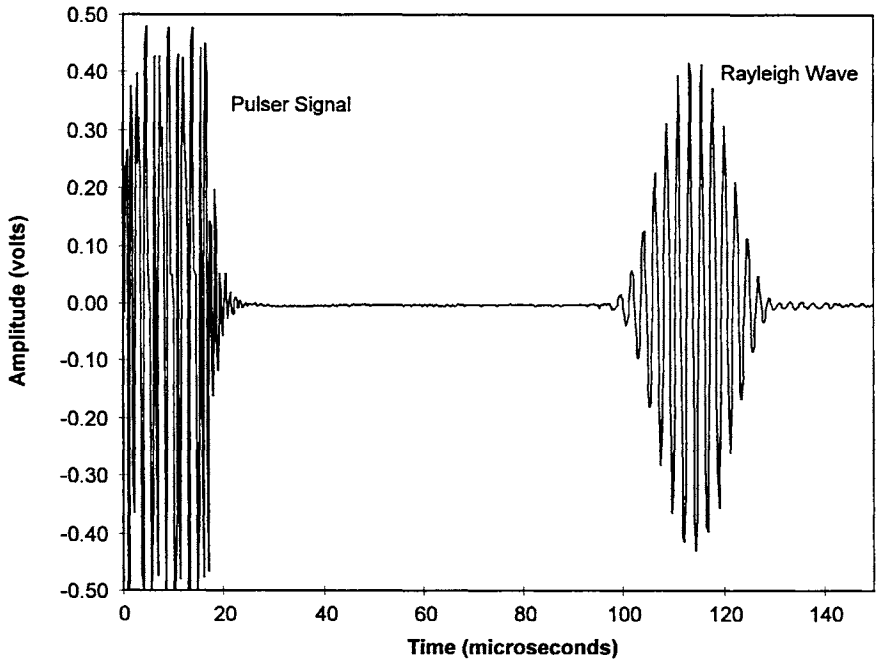

Figure 14. Strong Rayleigh wave signal through paint on bridge girder (lead-based paint/gain = 2)

Acoustic birefringence has a component B_o due to material texture (equation 4). To determine the stress, this must somehow be compensated for. In a bridge with only dead load stresses, the following scheme could be used. Assuming that the spans are simply supported, the shear stress will be zero at midspan by symmetry. Furthermore the (normal) bending stress will by definition vanish at the neutral axis. Consequently we could determine the texture component B_o by measuring the birefringence at this location. Previous measurements at NIST showed a high degree of homogeneity in rolled plate specimens of A-36 steel. The girder in the span we measured on the bridge was actually a rolled I-beam section. We knew that such sections might not be as homogeneous as rolled plate[10]. Hence the need to determine B_o on the actual bridge girders, as opposed to using the value of B_o measured on rolled plate.

However, the girders on the I-64 bridge were cambered to compensate for deadload deflections. Cambering causes residual stresses; the shear stresses will vanish at midspan since the camber is approximately symmetric. However, the normal stress due to cambering will not necessarily vanish at the neutral axis. Therefore we planned to measure B_o at the ends of the spans, which (according to the blueprints) extended about 150 mm (6 in) past the bearings. The bending and shear stress would vanish at this location, and near the bottom flange the (vertical) normal stress due to bearing reaction would also vanish. We planned to measure B_o at the bottom flange at the free ends of the beams. Comparison with B_o measured at opposite ends of the girders would then indicate the homogeneity of texture in the beam.

Unfortunately we discovered that the construction did not correspond to the blueprints. The bearings were placed directly under the ends of the girders, which caused a large normal stress acting in the vertical direction. This stress would not vanish at the ends of the girders, and it would be difficult to calculate its magnitude there. Consequently we were unable to directly determine B_o by direct measurement. However, we were able to use an approximation scheme to estimate B_o (see Appendix).

Measurements of birefringence were made at 51 mm (2 in) increments on several vertical scanlines on the web of one of the outer girders. The EMAT was used in conjunction with a holder to ensure proper placement. The holder has handles for ease of handling, and magnets which attach it to the vertical surface of the web. Placement took only a few seconds (Figure 15). There were grooves in the web (presumably as a result of

Figure 15. Shear wave EMAT attached to the vertical web surface

the rolling process), and in some cases the corresponding ultrasonic signal was weak, probably because the grooves scattered the ultrasonic beam. The signal was somewhat weaker than in laboratory tests made before the field test. The laboratory specimens were unpainted. Apparently the paint reduced the ultrasonic signals. The girders were painted with lead-based paint, which had a thickness of about 0.15-0.25 mm (0.006-0.01 in) on the web.

We were able to obtain reliable data at 11 locations on one vertical scanline in the web. We were unable to obtain data in the flanges. We used the approximation outlined in the Appendix to estimate the value of B_o for the web. Then we were able to convert our measured B to stress by using equation (4). This is given as σ_{xx} in Table A1 in the Appendix.

From the blueprints we were also able to determine the (linear) bending stress distribution due to the dead load of the deck and girder. The coverplate on the bottom flange shifted the neutral axis down about 150 mm (6 in) below the girder center. The peak stresses were about 126 MPa (compression) in the top flange and 63 MPa (tension) in the bottom flange. These calculated stresses were subtracted from the measured stresses to give the residual stresses due to cambering, etc. (Figure 16).

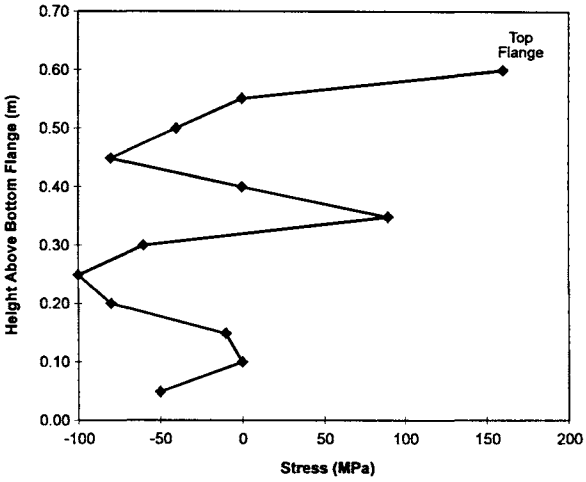

Figure 16. Residual stress distribution in the web.

Case 2: Rte. 257 Bridge over I-81

Applied Stresses

Stress measurements were performed on steel girders at the integral backwall bridge on Rte. 257 over I-81. Assistance in evaluating stresses was requested because resistance strain gages installed on-site indicated excessive stresses on the bottom flanges near abutment A. The backwall bridge was a fairly novel design, used to overcome problems associated with the presence of joints in conventional bridges (Figure 17).[20] It consisted of ten continuous girders supported at midspan by a pier located in the median of I-81. The ends of all girders were cast into the integral backwall, basically a reinforced concrete wall integral with the deck which tied all the girder ends together. Backwalls move against soil pressure, to accommodate changes in girder length due to thermal expansion. There were no expansion joints in the deck, and thus no way for road salt and other corrosion-causing agents to attack the bearings. There were three bearings per girder: one fixed bearing at the pier, and two expansion bearings at each backwall. Expansion bearings rested on the abutments.

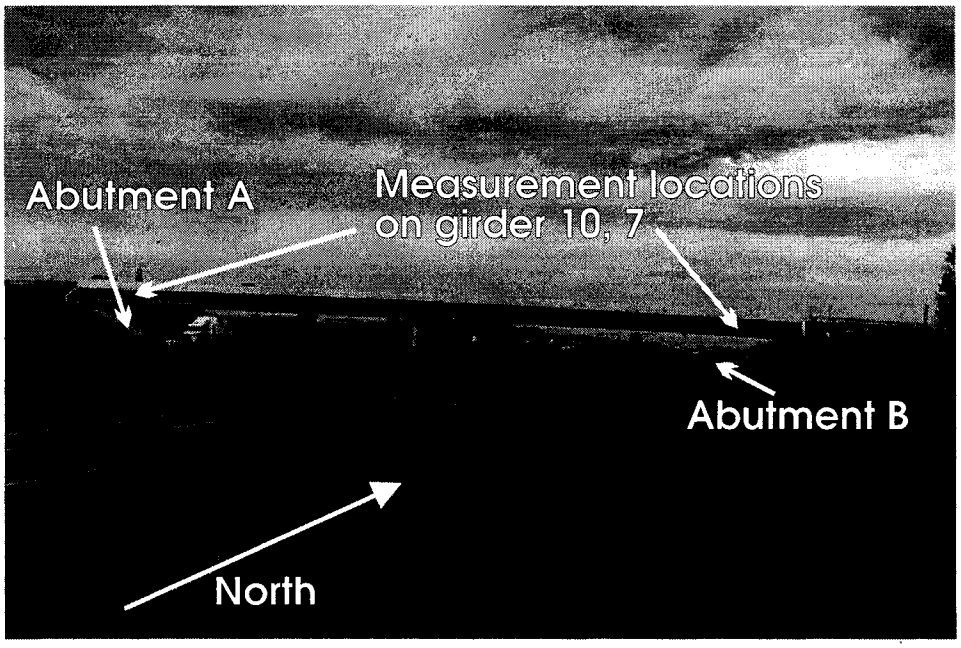

Figure 17. The Rte. 257 bridge over I-81.

As part of an ongoing research project, a variety of instruments had been installed to monitor the bridge.[20] There were strain gages on the bottom flanges of girders 10 and 7. The girders were numbered from north to south, making girder 10 the southernmost. The gages were located between the expansion bearings and the backwall. There were also strain gages on either side of the fixed bearings of girder 10 and girder 7 at the pier. The strain gages gave information about normal stress in the bottom flanges. This stress is due to at least two causes: in-plane bending, and axial compression. The latter could be caused if the thermal expansion was somehow impeded by, for example, bearing lockup. Tilt gages had also been installed on the pier and on girder 7. These monitored rotations of pier and girder. Pressure gages were also located behind the backwall and abutment at both sides of the bridge. Finally, there were gages at the pier to monitor the air temperature and steel temperature of girder 7.

Anomalous behavior was recorded by some of these gages. In particular, "spikes" indicating large compressive stresses were recorded by gages on girder 10 and girder 7 at abutment A. Some of these appear to have been real, because similar (but lower amplitude) spikes were recorded by strain gages at the pier. Some readings may be artifacts; in particular there were several occurrences where gages at abutment B indicated large step changes (of the order of 70 MPa or more) in compression with no corresponding changes in any of the other gages. A possible explanation was a dc offset problem in the instrumentation amplifiers. If the most recent readings in October are to be believed, there was about 350 MPa compression at abutment B. This was very close to the yield stress of the girders. If these readings were representative of the stresses in the girders in the region between the expansion and fixed bearings, buckling of the girders was also possible.

The bridge was on a 5 degree skew, so the centroids of soil pressure at abutments A and B were not collinear. An examination of the soil pressure records showed a *dc* component (in addition to the expected day-to-night oscillations). This could cause a rotation of the bridge over time, even allowing for the large mass moment of inertia of the bridge. Eventually some restoring moment will stop this rotation. This may result from bearing lockup (among other possible causes).

Improvements in ultrasonic equipment handling were subsequently made for this test. For proper grounding, the EMAT preamplifier needed to be grounded to the measurement girder (Figure 18). Using the 2 MHz EMAT, shear wave echoes were detectable in several areas of the girders without surface preparation. The bridge surface had two coats: a primer and a top zinc base coat with total thickness 0.15-0.50 mm (0.006-0.02 in). However, in other areas of the girders the signals were not present. When shear wave echoes were not detectable on an unprepared surface, the paint on the girder was removed. Sometimes the application of paint stripper, brushed lightly on the surface on material opposite the EMAT, was sufficient to get good echoes. Sometimes the paint needed to be removed directly below the EMAT.

Application of spray adhesives to the paint surface in an attempt to get good shear wave echoes was not successful. Materials like spray adhesive on the top coat of paint had no effect on the reflected shear waves at the interface of the primer and the top coat of paint. Good shear wave echoes were only obtained when the top coat of paint was altered or removed. Figure 19 shows examples of strong and weak EMAT signals; Table 2 lists surface preparations performed to improve the signals.

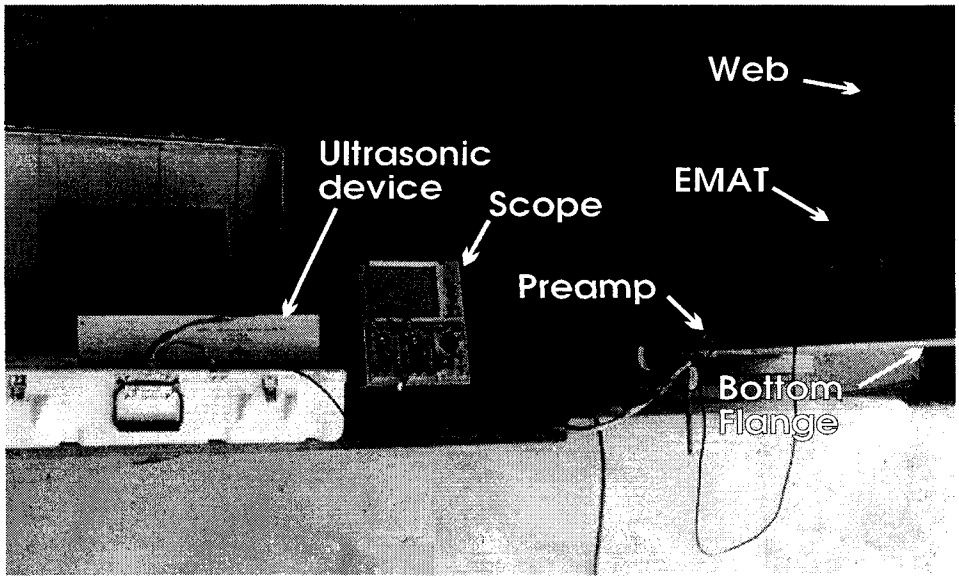

Figure 18. The EMAT attached to the web and preamplifier grounded to the girder.

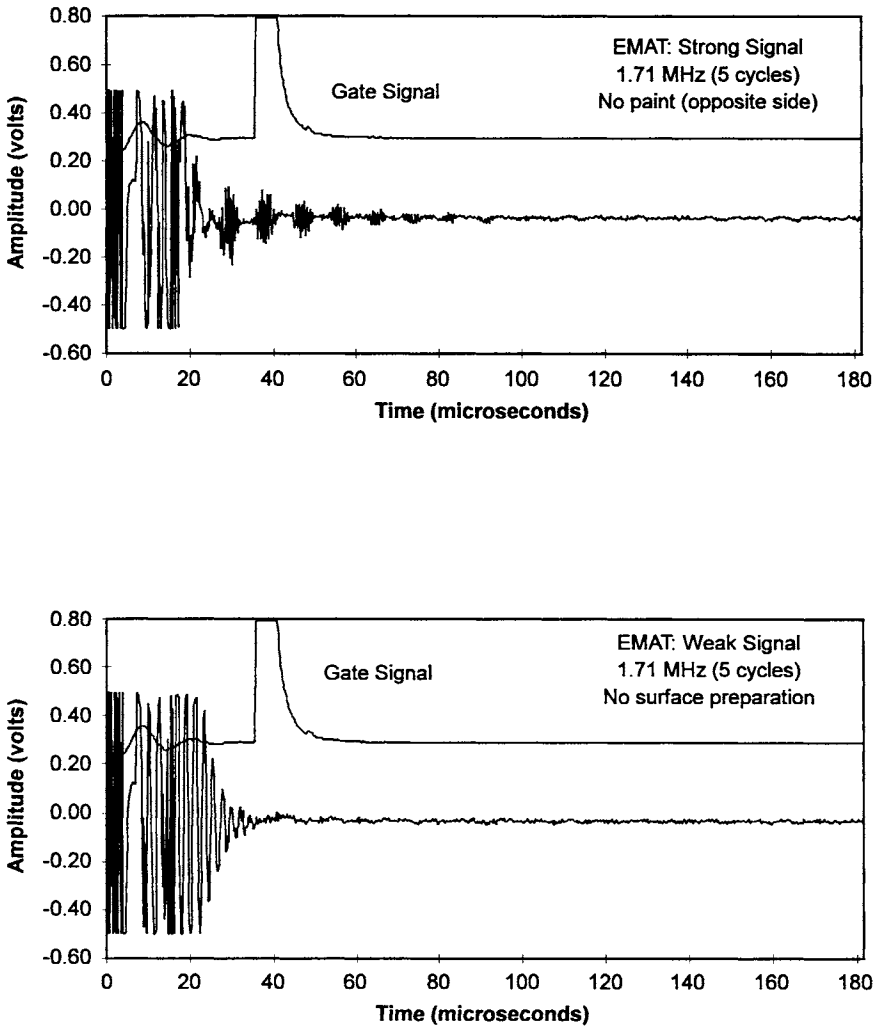

Figure 19. Strong and weak shear wave signals from EMATs.

Piezoelectric shear wave transducers were also used to compare the signal strength to the EMATs. Both a 2 MHz and a 5 MHz shear wave transducer were used. Honey was an effective couplant between the transducer and the material surface. When driving the 2 MHz transducer at frequency of 1.5 MHz, strong signals were seen at each location examined on the web and flanges. No locations were observed where the shear wave echoes were extinguished by the paint. With the 5 MHz transducer, most areas examined resulted in strong signals. However, there were some areas of weak signals. This supports the theory that changing the frequency of the shear waves changes the effect of paint on the received signals. Apparently, the 2 MHz transducer was operating at a good frequency for suppressing the effects of paint on the received signals. Figure 20 shows strong and weak signals from piezoelectric transducers.

Table 2. Surface Preparation for Signal Improvement

Location	Flange			
	Girder 10		Girder 7	
	Abutment A	Abutment B	Abutment A	Abutment B
	Preparation	Preparation	Preparation	Preparation
1	PRO	PRB	PBS	PRT
2	PBS	PRO	PBS	PRT
3	PRO	PRB	PRO	PBS
4	PRO	PBS	PRB	PBS
5	PRB	PRB	PRB	PRB
6	PRT	PBS	PBS	PRB
7	PRB	PBS	PBS	PBS
8	PRB	PBS	PRB	PBS
9	-	PBS	PRB	PBS
10	-	-	PRB	PBS
Web				
1	PBS	PRB	-	-
2	PBS	PRB	-	-
3	PBS	PRB	-	-
4	PBS	PRB	-	-
5	PBS	PBS	-	-
6	PBS	PBS	-	-
7	PBS	PBS	-	-
8	PBS	PBS	-	-
9	PBS	PBS	-	-
10	PBS	PRB	-	-
11	PBS	PRO	-	-
12	PBS	PBS	-	-
13	PBS	PBS	-	-

Legend: PBS=Paint on both sides of the member. The signal was strong and no surface preparation was performed.
PRT=Paint removed from the top surface, where transducer was placed. The signal was weak without surface preparation and became stronger after paint or paint+primer removal from the surface.
PRO=Paint removed from the opposite surface of the member, where transducer was placed. The signal was weak without the surface preparation and became stronger after paint or paint+primer removal from the opposite surface.
PRB=Paint removed from the both surfaces of the member. The signal was very weak without surface preparation and became stronger after paint or paint+primer removal from the both surfaces of the member.

Measurements were made first on the flange at several locations to determine the texture homogeneity (the stress is sensibly constant over the measurement region). This was done at both sides of the bridge at abutments A and B. Table 3 shows birefringence data taken in October and November 1995 on the flanges of the girders. Data were also taken with a piezoelectric transducer to compare with EMAT results.

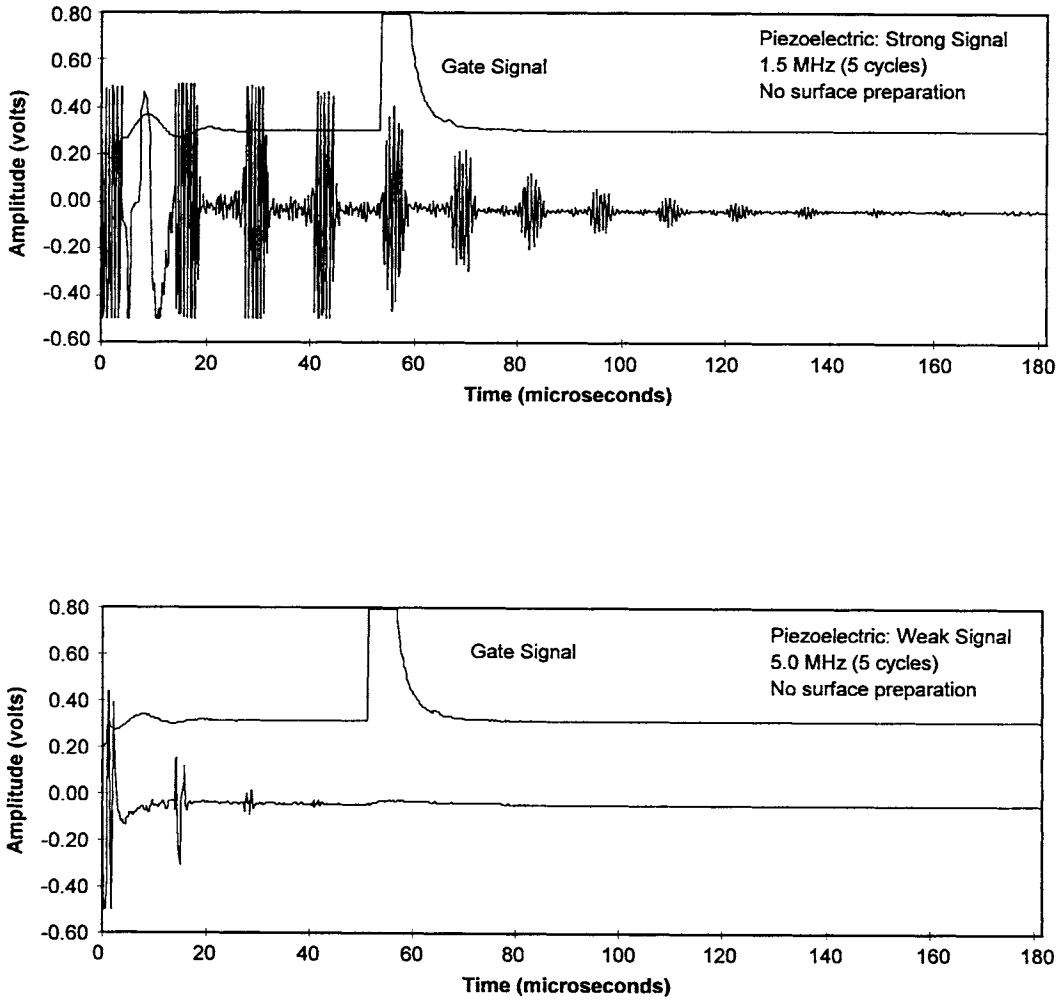

Figure 20. Strong and weak shear wave signals from piezoelectric transducers.

Table 3. Birefringence Data ($B_0 \times 10^{-3}$) Taken on the Flange of Girders 10 and 7

Location	Girder 10							
	October Test				November Test			
	EMATs		PIEZO		EMATs		PIEZO	
Abutment	Abutm A	Abutm B	Abutm A	Abutm B	Abutm A	Abutm B	Abutm A	Abutm B
1	2.78	-	-	-	2.56	-	2.71	-
2	2.89	2.62	-	-	2.45	-	2.59	-
3	2.78	2.34	2.86	2.64	2.34	-	2.22	-
4	3.15	3.05	-	-	2.46	2.21	2.83	2.47
5	2.86	2.47	-	-	-	-	-	-
6	3.14	2.58	-	-	2.78	2.38	2.64	2.21
7	2.92	2.58	-	-	-	2.41	-	2.35
8	2.86	2.74	2.78	-	-	2.45	-	2.31
9	-	2.27	-	2.38	-	2.11	-	2.32
10	-	-	-	-	-	-	-	-
Average	2.92	2.65	2.82	2.51	2.51	2.31	2.59	2.33
Std. Dev	0.15	0.31	0.06	0.09	0.17	0.15	0.22	0.09
Ave B - Ave A	-0.27		-0.31		-0.2		-0.26	
Ave B - Ave A, MPa	27		31		2		26	
Girder 7								
Location	October Test				November Test			
	EMATs		PIEZO		EMATs		PIEZO	
Abutment	Abutm A	Abutm B	Abutm A	Abutm B	Abutm A	Abutm B	Abutm A	Abutm B
1	2.76	1.85	-	-	2.33	1.67	2.59	2.21
2	2.61	1.89	-	-	2.52	1.98	2.88	1.87
3	2.88	1.76	-	-	-	-	-	-
4	2.76	1.95	-	-	2.63	1.79	2.85	2.34
5	2.8	1.89	-	-	-	-	-	-
6	2.62	1.73	-	-	2.61	1.85	2.81	2.09
7	3.12	2.12	-	-	2.79	1.77	2.77	2.12
8	3.34	2.01	-	-	-	-	-	-
9	2.9	1.91	-	-	2.53	1.98	2.85	2.19
10	2.87	1.91	-	-	-	-	-	-
Average	2.83	1.9	-	-	2.57	1.84	2.79	2.13
Std. Dev.	0.16	0.11	-	-	0.15	0.13	0.11	0.16
Ave B - Ave A	-0.93		-		-0.73		-0.66	
Ave B - Ave A, MPa	93		-		73		66	

In an attempt to determine the magnitudes of the bending and axial components, ultrasonic measurements were made not only on the bottom flange of girder 10 but also in the web at abutment A and B. If traditional beam theory applies to the in-plane bending component, then the stress distribution will have an average value (due to axial component) plus a linear component (due to bending). Measurements were made up the web with a separation distance of approximately 10 cm intervals until the midline of the web was reached. Then data were taken at 20 cm intervals in the top half of the girder. Shear stresses in the girder webs could cause rotation of the acoustic axes (directions of polarization of "fast" and "slow" shear waves). When good shear waves were present on the measurement surface, the birefringence rotation data were as expected and consistent with laboratory experiments. In practice the rolling direction (along the beam axis) was always the fast direction, within experimental error. It was estimated that the orientation of the acoustic axes could be determined to within about plus/minus 10 degrees. Figure 21 shows web birefringence data for abutment A and B of girder 10.

For these measurements the relation between birefringence and stress is

$$B = B_0 + C_a \sigma_{xx} \qquad (11)$$

where σ_{xx} is the normal stress (acting along beam axis) due to combined bending and tension.

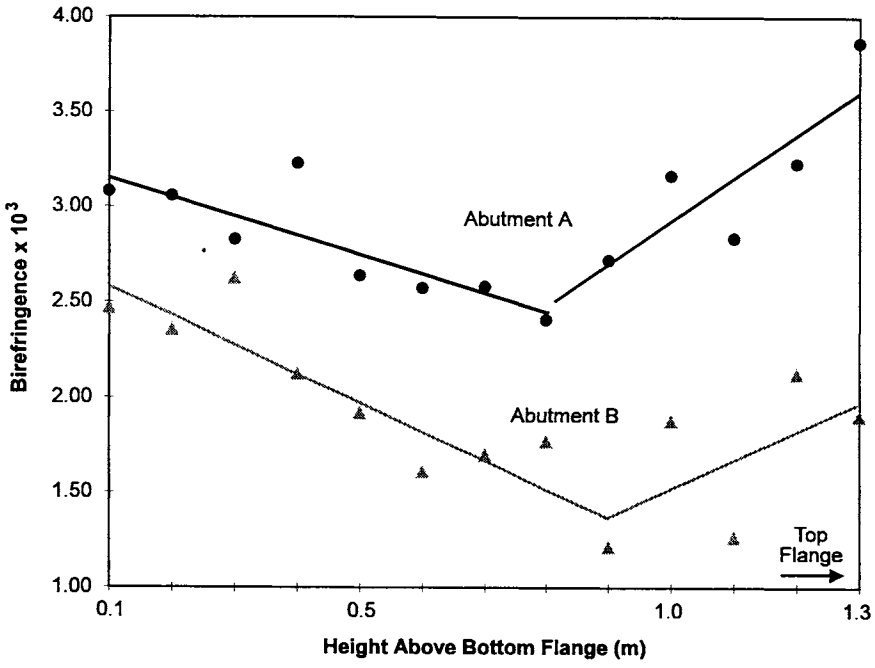

Figure 21. Web birefringence data (birefringence change 1 x 10^{-3} is equivalent to about 100 MPA)

B_0 is the value of B at a location of zero stress. There was no such location in the vicinity of the abutments; such a location existed at the neutral axis at the contraflexure points (where beam curvature is zero), somewhere over I-81.

Furthermore the EMATs measure the total state of stress, which includes any stresses due to welding, fabrication, cambering of beams, shrinkage of concrete deck, etc.; the dead load stresses; additional stresses due to shifting, rotation of abutments, etc.; and stresses due to thermal expansion being resisted by bearing lockup.

From the strain gages installed on girders 10 and 7, and the soil pressure and temperature gages, it appears that abutment B is well-behaved. There was a good correlation between various gages. Hence we propose to use acoustic data at this side of the bridge as a reference. That is, we will consider the difference in birefringence between abutment A and B, at the same elevation above the bottom flange.

In this way we subtract any stresses due to the first two causes listed above, leaving only stresses which could indicate a state of distress in the bridge. For example, Table 3 (flanges data only) also shows the results of subtracting the stress at abutment A from that at B. Table 4 shows corresponding data taken along the scanlines in the web. Note that the birefringence data for abutment A is always more positive than for abutment B. This indicates a higher average compression for girders at abutment A. The ultrasonic data suggest a difference of 20-30 MPa for girder 10 and 60-90 MPa for girder 7.

A measure of the expected accuracy of the stress results is given by

$$d\sigma = \frac{dB_r}{C_a} \qquad (12)$$

where $d\sigma$ is the stress uncertainty, dB_r is the birefringence standard deviation, and C_a is the stress-acoustic constant. The maximum stress uncertainty $d\sigma$ calculated in this way was about 30 MPa, quite acceptable for our application.

When the strain gage dataloger that indicated large compressive flange stresses at abutment A was replaced, the stresses at abutment A were similar to those at abutment B.[21] The ultrasonic data indicated that the flange stress at abutment A was more compressive than abutment B. This is within the measurement uncertainty of about plus/minus 30 MPa due to texture variations in the steel.

The stresses measured here are on the opposite side of the bearing from the strain gages. If there is bearing lockup, then there will be a possible discontinuity in stresses across the bearing. It will be useful to return to the bridge and measure the stresses between the bearing and

backwall. The question of texture homogeneity is still open. One way to suppress the texture problem is to use grazing shear waves, if they are not severely attenuated by paint.

Table 4. Birefringence Data ($B_0 \times 10^{-3}$) Taken on the Web of Girder 10

Web Vertical Distance, m	Abutment A	Abutment B
0.1	3.08	2.47
0.2	3.06	2.35
0.3	2.83	2.62
0.4	3.23	2.12
0.5	2.64	1.92
0.6	2.57	1.61
0.7	2.58	1.7
0.8	2.41	1.77
0.9	2.72	1.21
1	3.16	1.88
1.2	2.84	1.26
1.4	3.23	2.12
1.5	3.87	1.9

SUMMARY

Live load measurements were made by determining the normalized change in arrival times of surface waves propagating between two transducers mounted on the bottom flange of the simply supported girder.

Strain gages were mounted on the flanges for comparison with ultrasonic live load measurement. A test vehicle was driven over the bridge at a range of speeds from 8 to 90 kmph (5 to 55 mph). Good agreement between strain gage and ultrasonic data was obtained, both for the time-history of strain and also for the equivalent stress range.

The ultrasonic equipment for live load measurements is portable and easily installed. Measurements were made without paint removal, in contrast to strain gage installation.

Residual stress measurements were made on a vertical scanline in the web at midspan where the maximum dead load bending stress occurs. There will also be residual stresses from rolling of the girder during manufacture and stresses from cambering the girders before the deck is poured.

Residual stress measurements were made of the phases of shear waves propagating through the web; the waves were polarized in rolling and transverse (vertical) directions. However, the bearings were placed at the girder ends, so we resorted to an approximate scheme to obtain birefringence in the unstressed state. We required that the stress give zero net axial force. With birefringence in the unstressed state determined, we then calculated the total bending stresses σ_{xx} in the web from the birefringence data. To obtain the residual stress we subtracted the calculated dead load bending stress.

On the integral backwall bridge, previously installed strain gage instrumentation indicated a difference of over 350 MPa from one side of the bridge to the other. It was suspected that one set of instrumentation electronics was malfunctioning.

Stress measurements were made with ultrasonics at web and flange locations at both sides of the bridge. The stress data at abutment A were subtracted from those at abutment B. In principle, the difference relates to any additional stress possibly caused by superstructure rotation and/or bearing lockup.

The data reduction scheme resulted in a bending component and a constant component (non-zero net axial force). The magnitude of the former is what would result from a 0.5 degree rotation of the backwall (top tilts toward pier). The constant stress was about 60-70 MPa.

After the electronics that indicated large compressive flange stresses at abutment A were replaced, the stresses at abutment A were similar to those at abutment B. The ultrasonic data indicated that the flange stress in the outer girder at abutment A was about 30 MPa more compressive than at abutment B. This is within the measurement uncertainty of about plus/minus 30 MPa, due to texture variations in the steel.

RECOMMENDATIONS FOR FURTHER RESEARCH

Nondestructive evaluation of the stresses in steel bridges should include using EMATs to:

- Monitor steel bridges with existing fatigue cracks to obtain loading histories and study discrimination between acoustic signals during loading.
- Study the effects of paint and surface texture during stress measurements by using EMAT for surface-skimming shear waves.

- Apply NDE stress measurements to pin and hanger assemblies. Calculations have shown that large bending stresses occur in the hanger if the pin is frozen. These stresses can be determined by measuring the birefringence on opposite sides of the hanger at midsection. The difference is proportional to the bending stress, which can be related to the shear stress in the pin. This technique should be easier than measuring the shear stress in the pin directly with ultrasonics.

ACKNOWLEDGMENTS

Thanks are due to H. I. McHenry of NIST, who authorized transferring the NIST stress measurement capability to VTRC, and H. GangaRao of the Constructed Facilities Center, West Virginia University, who agreed to demonstrate the fatigue loading indicator. We are grateful for many suggestions and discussions from G. A. Alers of NIST on various aspects of operation of the EMATs. S. R. Schaps of NIST designed the preamplifiers, which were built by R. Santoya. R. E. Schramm and T. Nguyen of NIST assisted with equipment checkout prior to the field test. P. A. Fuchs acknowledges the financial support of the FHWA. G. R. Allen, M. M. Sprinkel, E. J. Hoppe, J. P. Gomez and P. Massarelli of the Research Council reviewed the work and suggested improvements. Thanks are due to E. Yong, R. Tressell of VDOT, C. Apusen, J. French, A. French, M. Powell and C. Mai of VTRC for their assistance with various phases of the project, and to R. Combs and E. Deasy for assistance with the graphics and photographs. G. Mawyer edited the report.

REFERENCES

1. *Bulletin, A VDOT monthly newspaper*, Vol. 60, No. 6, June 1994.

2. Fisher, J. W. 1984. *Fatigue and fracture in steel bridges*. New York: John Wiley & Sons.

3. McKeel, W. T., Maddox, C. E., Kinnier, H. L., and Galambos, C. F. 1972. Loading history study of two highway bridges in Virginia. *Highway Research Record*, No. 382. Highway Research Board.

4. James, M. R., and Cohen, J. B. 1980. The measurement of residual stresses by X-ray diffraction techniques. *Treatise on Materials Science and Technology*, Vol. 19A, pp. 1-62.

5. Allen, A., Andreani, C., Hutchings, M. T., and Windsor, C. C. 1981. Measurement of internal stress within bulk materials using neutron diffraction. *NDT International*, Vol. 14, No. 5, pp. 24-28.

6. Burkhardt, G. L., Beissner, R. E., Matzkanin, G. A., and King, J .D. 1982. Acoustic methods for obtaining Barkhausen noise stress measurements. *Materials Evaluation*, Vol. 40, No. 6, pp. 669-675.

7. Kwun, H. 1986. A nondestructive measurement of residual bulk stresses in welded steel specimens by use of magnetically induced velocity changes for ultrasonic waves. *Materials Evaluation*, Vol. 44, No. 12, pp. 1560-1566.

8. Allen, D. R., Cooper, W. H. B., Sayers, C. M., and Silk, M. G. 1982. The use of ultrasonics to measure residual stresses. In *Research Techniques in Nondestructive Testing*, ed. R.S. Sharpe. New York: Academic Press, pp. 152-209.

9. Thompson, R. B., Lu, W.-Y., and Clark, Jr., A. V. 1995. Ultrasonic methods. In *SEM Monograph on Techniques for Residual Stress Measurement*. New York: SEM, in press.

10. Clark, A. V., and Schaps, S. R. 1995. Acoustoelastic determination of residual stress by measurement of resonance peaks and phase shifts. Submitted to *Journal of Nondestructive Evaluation*.

11. Alers, G. A., and Manzanares, A. 1990. Use of surface skimming SH waves to measure thermal and residual stresses in installed railroad tracks. In *Review of Progress in Quantitative Nondestructive Evaluation*. New York: Plenum, pp. 1757-1764.

12. Fuchs, P., Petro, S., Klinkhachorn, P., Halabe, U., GangaRao, H., and Chase, S. B. 1994. Fatigue loading indicator for bridges. In *Structural Materials Technology -- An NDT Conference*. Lancaster: Technomic, pp. 292-296.

13. Fuchs, P., Clark, A. V., and Schaps, S. R. 1995. Applied stress measurement in steel for fatigue load monitoring. In *Review of Progress in Quantitative Nondestructive Evaluation.* New York: Plenum, pp. 2153-2160.

14. Mandracchia, E. A. 1995. Ultrasonic measurements of applied stress in structural members. In *Nondestructive Evaluation of Aging Bridges and Highways.* Bellingham: SPIE, pp. 308-312.

15. Clark, A. V., Fuchs, P., and Schaps, S. R. 1996. Fatigue load monitoring in steel bridges with Rayleigh waves. In press, *Journal of Nondestructive Evaluation.*

16. Fuchs, P. A., Clark, A. V., and Schaps, S. R. 1995. Monitoring bridge fatigue loads with ultrasonic transducers. *Sensors-- The Journal of Applied Sensing Technology*, Vol. 12, No. 11, pp. 20-26.

17. Fuchs, P. A., et al., 1996. Field test results of an ultrasonic applied stress measurement system for fatigue load monitoring. In Press, *Structural Materials Technology -- An NDT Conference.* Lancaster: Technomic.

18. Fuchs, P. A., et al., 1996. Fatigue load monitoring system for bridges using EMATs. *FHWA Report.* Morgantown, WV: University of West Virginia.

19. Clark, A. V., and Anderson, T. L. 1996. Quantitative bridge safety assessment utilizing fracture mechanics and ultrasonic stress measurements. In press, *Structural Materials Technology -- An NDT Conference.* Lancaster: Technomic.

20. Hoppe, E. J., and Gomez, J. P. 1996. Field study of an integral backwall bridge. In preparation. Charlottesville: Virginia Transportation Research Council.

21. Hoppe, E. J., and Gomez, J. P. 1995. Personal communication. *Virginia Transportation Research Council.*

APPENDIX

Measurement of Birefringence

For the I-64 bridge measurements were made where the shear stress is zero. Then

$$B = \frac{(P_s - P_f)}{P} = B_0 + C_a(\sigma_f + \sigma_s) \qquad \text{(A1)}$$

where σ_f is normal stress acting in the fast direction, etc. We found that the slow direction corresponded to the rolling (x-) direction (along girder axis). Since C_a is negative we have

$$B - B_0 = -C_a \sigma_{xx} \qquad \text{(A2)}$$

For the backwall bridge there will be some shear stress σ_{xy} since measurements were made close to the bearings. These would in general cause rotations of the pure-mode polarization directions of the shear waves. The rotation of these directions relative to the rolling direction of the plate girders is given by

$$\tan(2\Theta) = \frac{2C_a \sigma_{xy}}{B_0} + C_a(\sigma_{xx} - \sigma_{yy}) \qquad \text{(A3)}$$

the relation between B and stresses becomes

$$B^2 = (B_0 + C_a(\sigma_{xx} - \sigma_{yy}))^2 + (2C_a \sigma_{xy})^2 \qquad \text{(A4)}$$

To determine the normal stresses we combine the above using trig identities to obtain

$$B\cos(2\Theta) - B_0 = C_a(\sigma_{xx} - \sigma_{yy}) \qquad \text{(A5)}$$

Since we measure at some distance from bearing we assume σ_{yy} vanishes.

For the backwall bridge we used abutment B as a reference. The strain gages indicated a small (less than 15 MPa) stress σ_{xx} there on the bottom flange. We therefore assume we can measure B_o there to within our experimental error. (On the bottom flange we have boundary

conditions $\sigma_{xy} = \sigma_{yy} = 0$). We also measured Bo on the bottom of the web, in case the texture might be different for flange and web. In fact these values were close to one another.

Since the rolling direction was the fast direction we have

$$B\cos(2\theta) - B_0 = C_a \sigma_{xx} \qquad \text{(A6)}$$

for the backwall bridge. In fact our measurements showed that to within experimental error $\Theta = 0$.

Estimate of *Bo* in Web of I-64 Bridge

We assume that the bearings are properly functioning so there is no net axial force. Then the integral of σ_{xx} over girder cross-section vanishes. From equation (A2) we then have

$$B_0 = \frac{1}{A_w}\left[\iint_{web} B\,dA + \iint_{flange} C_a \sigma_{xx}\,dA\right] \qquad \text{(A7)}$$

The first integral is evaluated from the measured birefringence in the web. Values of B are given in Table A1 below. To evaluate the second we need an estimate of σ_{xx} in the flanges.

Table A1. Values of Birefringence and Stress in Web

Location	B (10^3)	σ_{xx} (MPa)	$\sigma_{xx,r}$ (MPa)
2	5.3	100	160
3	3.5	-80	0
4	3.3	-100	-40
5	2.8	-150	-80
6			0
7	4.9	60	90
8	3.5	-80	-60
9	3.1	-120	-100
10	3.4	-90	-80
11	4.3	0	-10
12	4.5	20	0
13	4.4	10	-50

We assume negligible residual stress in flanges; then stresses there are due to dead load. We calculated these dead load stresses as outlined in "Calculation of Deadload Stresses." Upon substitution of these into the second integral above we find $B_0 = 4.3(10^{-3})$.

Calculation of Deadload Stresses

The bridge has a simply supported span 24 m (75 ft) long carrying a uniform load P lbs/ft. The bending moment at midspan is $PL^{2/8}$ from beam theory. The corresponding bending stress

$$\sigma_{xx'b} = M(\frac{y}{I}) \qquad \text{(A8)}$$

where y is the distance from neutral axis and I is the area moment of inertia.

The girder is a 36 WF 182 section with coverplate 37 mm (1.5 in) thick and 262 mm (10.5 in) wide. Using beam dimensions we find that the coverplate causes the neutral axis to be 135 mm (5.6 in) below girder center. The corresponding I is about 250^4 mm^4 (10^4 in^4).

The deck thickness is 200 mm (8 in) and the girder carries a width of about 2.4 m (8 ft) of deck. For nominal concrete density of 2.3 kg/cm^3 (150 lb/ft^3) we have P = 1500 kg/m (1 kip/ft). The bending stresses in the flanges are then about 126 MPa (upper) and 63 MPa (lower).

Calculation of Residual Stresses

We use the values of birefringence from Table A1 above (plus the value of B_0) in Equation 2 to calculate the total stress σ_{xx} (the third column in Table A1). We then subtract the calculated deadload stresses from these to determine residual stress $\sigma_{xx,r}$ in the web (fourth column in Table A1).

To estimate $\sigma_{xx,r}$ in flanges we use the following equations

$$\iint \sigma_{xx',r}\, dA = 0 \qquad \text{(A9)}$$

$$\iint y\, \sigma_{xx',r}\, dA = 0 \qquad \text{(A10)}$$

which result from the fact that $\sigma_{xx,r}$ is self-equilibrating. The integral over the web area are evaluated using values of $\sigma_{xx,r}$ from Table 1. We assume $\sigma_{xx,r}$ has constant values $\sigma_{xx,ruf}$ and $\sigma_{xx,rlf}$ in upper and lower flanges. Then we solve the above equations get $\sigma_{xx,ruf} = -17$ MPa, $\sigma_{xx,rlf} = 6$ MPa.